Eur. J. Mineral.
2004, **16**, 99-110

Potential problems in the interpretation of powder X-ray diffraction patterns from fine-dispersed $2M_1$ and $3T$ dioctahedral micas

VICTOR A. DRITS* and BORIS A. SAKHAROV

Geological Institute, Russian Academy of Sciences, 7 Pyzhevsky Street, 119017 Moscow, Russia

Abstract: XRD patterns were calculated for $2M_1$ and $3T$ dioctahedral mica structural models in which *trans*-vacant (*tv*) and *cis*-vacant (*cv*) layers were interstratified and arranged, independent of octahedral cation distribution, as in the periodic $2M_1$ and $3T$ mica polytypes. The XRD patterns of the interstratified *cv*/*tv*$2M_1$ and *cv*/*tv*$3T$ models were shown to be similar to those of the *tv*$2M_1$ and *tv*$3T$ mica structures, respectively. Because both the positions and shapes of *hkl* reflections in the XRD patterns of the *tv*$3T$ and *cv*/*tv*$3T$ as well as of the *tv*$2M_1$ and *cv*/*tv*$2M_1$, respectively, are the same qualitative X-ray identification of the *tv*$2M_1$, *cv*/*tv*$2M_1$, *tv*$3T$ and *cv*/*tv*$3T$ mica varieties should be a complex problem, especially when the amount of *cv* layers is either rather low (10-15 %) or high (30-40 %) with significant tendency to segregation of the layer types.

The diffraction features of *cv*/*tv*$2M_1$ and *cv*/*tv*$3T$ mica structures make it possible to use the Rietveld technique for the structural refinement. Correct application of this technique to the *cv*/*tv*$2M_1$ and *cv*/*tv*$3T$ structures should reveal partial occupancy of *trans*-octahedra because of the ability of diffraction to average structural parameters. Pavese *et al.* (2001) found partial occupancies of *trans*-octahedra in $3T$ and $2M_1$ powder phengite samples. To explain these results the authors postulated the $\pm b/3$ stacking disorder. However, the calculations have shown that such disorder strongly modifies the XRD patterns. Therefore, in the paper an alternative, crystal-chemically more justified hypothesis is suggested according to which the occupancy of *trans*-sites in $3T$ and $2M_1$ phengites results from coexistence of *tv* and *cv* layers in their structures. Diffraction features a dioctahedral mica sample given as a *tv*$3T$ standard in textbooks (Brindley, 1980; Bailey, 1984) are quite similar to those characteristic for a $3T$ structure in which *tv* and *cv* 2:1 layers are interstratified.

Key-words: *cis*-vacant layers, *trans*-vacant layers, $\pm b/3$ disorder, interstratification, $2M_1$, $3T$ mica polytypes, simulation of XRD patterns.

1. Introduction

Micas are rock-forming minerals which occur in quite different geological environments and are often used as markers of metamorphic grade. The mica structure consists of 2:1 layers separated by large interlayer cations, such as K or Na. In the general case, the octahedral sheet of a 2:1 layer contains three symmetrically independent sites differing in mutual dispositions of OH groups and oxygen atoms coordinating octahedral cations. They are termed as M1 or *trans*-sites, and M2 and M2', or *cis*-sites.

For a long time it was commonly accepted that in dioctahedral phyllosilicates and in micas, in particular, the *trans*-sites are vacant. This supposition was based on single crystal structural refinements where octahedral cations in 2:1 layers of various polytypes of muscovite, phengite, paragonite and margarite were shown to occupy only *cis*-sites (Bailey, 1984). Therefore, identification of fine dispersed mica polytypes and illites, in particular, was usually based on the comparison between experimental positions and intensities of *hkl* reflections and those calculated for *trans*-vacant (*tv*) polytype structural models given in reference books (Brindley, 1980; Bailey, 1984).

The existence of dioctahedral phyllosilicates with different distributions of octahedral cations was first reported by Méring & Oberlin (1967) for a sample of Wyoming montmorillonite, for which one of the two symmetrically independent *cis*-octahedra of the 2:1 layer was shown to be vacant. Drits *et al.* (1984) deduced unit cell parameters and atomic coordinates for a one-layer monoclinic *cis*-vacant (*cv*) illite model (*cv*1*M*). These authors calculated powder XRD patterns for periodic *cv*1*M* and *tv*1*M* models, as well as for models in which *cv* and *tv* mica-like layers are interstratified. Based on these data they formulated diffraction criteria for identification of the periodic and interstratified mica-like structures as well as for those containing rotational stacking faults. Zvyagin *et al.* (1985) were the first to describe a monomineral Al-rich *cv*1*M* mica sample. Reynolds & Thompson (1993) and Drits *et al.* (1993) described other occurrences of *cv*1*M* illites. The state of the

*E-mail: dritsva@geo.tv-sign.ru

DOI: 10.1127/0935-1221/2004/0016-0099

0935-1221/04/0016-0099 $ 5.40

art in structural and crystallochemical study of micas was recently presented by Brigatti & Guggenheim (2000).

Tsipursky & Drits (1984), using oblique-texture electron diffraction (OTED), showed that dioctahedral smectites have a wide range of proportions of *cv* and *tv* layers. Reynolds (1993), McCarty & Reynolds (1995) and Drits *et al.* (1996) demonstrated that the *cv* structure exists in illite fundamental particles of the mixed-layer illite-smectites (I-S) exhibiting the 1*M* and 1*Md* stacking sequences, and that *cv* 2:1 layers are commonly interstratified with *tv* layers in these illite stackings. Coexistence of *cv* and *tv* layers in I-S formed in volcanic and sedimentary rocks was recently described in many papers (McCarty & Reynolds, 2001; Drits *et al.*, 1998a, 2002; Ylagan *et al.*, 2000; Lindgreen *et al.*, 2000; Cuadros & Altaner, 1998). Drits & McCarty (1996) proposed a method for semiquantitative determination of coexisting *tv* and *cv* layers in 1*M* illite and I-S using experimental d(11*l*) values.

Drits *et al.* (1993) noted that *tv*3*T* and *cv*1*M* mica polymorphs produce similar diffraction effects, that is, in their XRD patterns *hkl* reflections have similar intensities and close positions. These features explain the reason for confusion in the identification of *tv*3*T* illite. Careful analysis of the experimental data published in the literature showed that illite varieties described as 3*T* (Warshaw, 1959; Ey, 1984; Halter, 1988) in fact, correspond to *cv*1*M* (Drits *et al.*, 1993). Additional problems with reliable identification of the actual structure of illites and other fine dispersed dioctahedral micas may arise because of the similarity of XRD patterns corresponding to different mica varieties. For example, coexistence of *tv* and *cv* layers was found in a nonswelling illite sample from Amethyst Vein system, Creede Mining District, Colorado (Drits & McCarty, 1996) which was initially described as 3*T* illite (Horton, 1983). The reason is that powder XRD patterns corresponding to *tv*3*T*, *cv*1*M* and interstratification of *tv* and *cv* layers in 1*M*d illite in which *cv* layers prevail are very similar.

Recently Pavese *et al.* (2001) studied 3*T* and $2M_1$ powder phengite samples using low-temperature neutron diffraction and the Rietveld technique. Phengites have the idealized composition $K(Al_{1.5}Mg_{0.5})(Si_{3.5}Al_{0.5})O_{10}(OH)_2$ and attract special attention because crystallization of a specific polytype is supposed to depend on the thermobaric conditions, which, in their turn, control the cation ordering occurring in tetrahedral and octahedral sheets of the 2:1 layers (Sassi *et al.*, 1994). For the studied 3*T* and $2M_1$ samples Pavese *et al.* (2001) found that the occupancies of *trans*-octahedra of these micas are not zero but roughly equal to 0.18 and 0.12 atoms per octahedron, respectively. The title of their paper contains a question: are these occupancies real or an artefact? To explain the observed results, Pavese *et al.* (2001) postulated stacking disorder resulting from ± *b*/3 slips in the octahedral sheet of the 2:1 layer that occur in $2M_1$ and 3*T* phengites. At the same time, the authors noted that the ± *b*/3 disorder was observed experimentally only for trioctahedral micas (Noe & Veblen, 1999), as for dioctahedral micas, there are energy hindrances against this type of disorder. One has to note that a partial occupancy of *trans*-sites in Mg-Fe-bearing muscovites $2M_1$ was determined by Brigatti *et al.* (1998, 2000).

Taking into account that interstratification of *tv* and *cv* layers in illite stacking sequences exists, one may assume that the occupancy of *trans*-sites found in 3*T* and $2M_1$ phengite samples results from coexistence of both layer types in their structure. The main aim of this paper is to consider this alternative hypothesis using simulation of powder XRD patterns from different structural models. Special attention is paid to potential problems related with identification of dispersed dioctahedral mica varieties based on their powder XRD patterns.

2. Simulation of XRD patterns

The presence of stacking faults often prevents crystal-chemical studies of dispersed layer minerals by conventional methods of structure analysis, including the Rietveld technique. One of the effective ways to obtain structural and crystal chemical information from such minerals is to simulate diffraction effects from realistic structural models and then to compare the calculated and experimental XRD patterns (Drits & Tchoubar, 1990). This approach was successfully applied to natural and synthetic phyllosilicates (Sakharov *et al.*, 1990; Plançon *et al.*, 1989; Reynolds, 1993; McCarty & Reynolds, 1995, 2001; Manceau *et al.*, 2000; Drits *et al.*, 1993) and phyllomanganates (Drits *et al.*, 1998b; Lanson *et al.*, 2000, 2002; Manceau *et al.*, 1997). The mathematical formalism used to calculate powder diffraction patterns was described by Plançon & Tchoubar (1977), Plançon (1981), Sakharov *et al.* (1982) and, in greater detail, by Drits & Tchoubar (1990). One of the main advantages of this approach is that it can predict diffraction effects from diverse, theoretically possible and crystal chemically justified layer structural models. Its application makes it possible to analyze diffraction effects of various parameters describing specific features of periodic and defective structural models. For each particular model, the following structural and probability parameters should be defined: the structure and chemical composition of coexisting layers; the azimuthial orientations, translations, reflection operations and modes of alternation of the layers; probability parameters that describe quantitatively the model (*e.g.* proportion of each layer type, W_i, and conditional probability, P_{ij}, denoting the probability of a layer type j to follow layer type i, when the short-range factor is equal to 1). It is assumed that the interstratification of the layer types follows the Marcovian statistics (Drits & Tchoubar, 1990).

3. Structural models

Cartesian coordinates and parameters for the *cv* and *tv* unit cells used in this study are taken from Drits *et al.* (1984) and correspond to their designation of C and T layers. Let us term C^r and C^l the *cv* layers in which the fractional x, y coordinates of their vacant sites in the projection on the *ab* plane are equal to (0.346, – 0.333) and (0.346,

0.333) respectively. In the notation of Zvyagin (2001) C^r and C^l layers are denoted as 51 and 15, respectively. These numbers correspond to intersheet displacements S_iS_j characterized by their normal projections on the *ab* plane in the fixed coordinate system. These displacement vectors are relating the upward succeeding sheets TO and OT in a 2:1 layer, respectively. The origins of the tetrahedral sheets are in the centers of the ditrigonal cavities and the origins of the octahedral sheets are in the centers of vacant octahedra. The unit cells of the C^r, C^l and T layers have the same dimensions a = 5.200 Å, b = 9.007 Å, $a\sqrt{3}$, c^* = 9.98 Å and the same cation composition $K_{0.8}(Al_{1.70}\ Mg_{0.30})(Si_{3.5}\ Al_{0.5})\ O_{10}\ (OH)_2$. In projection on the *ab* plane, the position of K cation located in the ditrigonal hole of the upper tetrahedral sheet of the 2:1 layer is shifted with respect to the closest K site located in the lower tetrahedral sheet by – 0.383a and – 0.3085a along the a axis for the *tv* and *cv* unit cells, respectively.

3.1 The ± *b*/3 disordered model

In accordance with Nespolo (2001) and Nespolo & Ferraris (2001), Pavese *et al.* (2001) assumed that stacking disorder occurring in phengite samples consists in ± *b*/3 slips in the octahedral sheets of their 2:1 layers. These slips move the upper plane of the apical oxygen atoms with respect to the lower plane in the octahedral sheet. In order to preserve the octahedral coordination for interlayer K cations, the ± *b*/3 shift in the n^{th} layer requires the same shift for the layer located just above it. As a result, in dioctahedral micas the position of a filled *cis*-site is superposed on to that corresponding to a vacant *trans*-site in the defect-free structure.

If all layers have the same azimuthual orientation, then five types of 2:1 layers are required to describe the ± *b*/3 disordered structural model. Along with a defect-free T layer, they include two "defective" layers, in which their upper parts including the upper plane of the apical oxygen atoms of the octahedral sheets are shifted with respect to the lower planes by + *b*/3 (T^u_+ layer) or – *b*/3 (T^u_- layer) along the b axis, respectively. Atomic coordinates for T^u_+ and T^u_- layers are obtained by adding and substracting 0.333b from the Y-coordinates of atoms located above the octahedral cation plane in T layer, respectively. For the next two defective layers in which their lower parts are shifted with respect to the upper one by + *b*/3 and – *b*/3, (T^l_+ and T^l_- layers), respectively, the 0.333b value is added and subtracted from the Y-coordinates of atoms located below the octahedral cation plane. To preserve the octahedral coordination of interlayer K cations some layer pairs must be excluded from the consideration and only the following pairs may exist:

$$TT;\ TT^u_+;\ TT^u_-;\ T^l_+T;\ T^l_-T;\ T^u_+T^l_+;\ T^u_+T^l_-;\ T^l_+T^u_+;\ T^l_+T^u_-;\ T^l_-T^u_+;\ T^l_-T^u_- \text{ and } T^u_-T^l_-.$$

The layer pairs having the same upper indexes but different lower ones (*e.g.* TT^u_+ and TT^u_-; $T^u_+T^l_+$ and $T^u_-T^l_-$) can be shown to be equivalent from the diffraction point of view. Therefore, to describe the ± *b*/3 stacking disorder in *tv*1*M* structure, three layer types, T, T^u_+ and T^l_+ or T, T^u_- and T^l_- can be used. For simplicity, the lower subindexes in the layer symbols may be omitted.

Table 1. Matrice of conditional probabilities for the ±*b*/3 disordered $2M_1$ models.

	T_{60}	T_{-60}	T^u_{60}	T^u_{-60}	T^l_{60}	T^l_{-60}
T_{60}	0	P	0	1-P	0	0
T_{-60}	P	0	1-P	0	0	0
T^u_{60}	0	0	0	0	0	1
T^u_{-60}	0	0	0	0	1	0
T^l_{60}	0	P	0	1-P	0	0
T^l_{-60}	P	0	1-P	0	0	0

For a defective $2M_1$ structure, adjacent layers should be rotated with respect to each other by ± 120° or related by glide plane as in the periodic *tv*$2M_1$ mica. Therefore, six layer types, T_{60}, T_{-60}, T^u_{60}, T^u_{-60}, T^l_{60} and T^l_{-60} should be used to describe the ± *b*/3 stacking sequence in defective $2M_1$ micas. Lower indices 60 and –60 correspond to rotations of T, T^u and T^l layers by 60° counter-clockwise and clockwise, respectively, relative to the fixed a axis. One may assume that the occurrence probabilities $W(T_{60}) = W(T_{-60}) = W$ and $W(T^u_{60}) = W(T^u_{-60}) = W(T^l_{60}) = W(T^l_{-60}) = W_i$. Table 1 shows that among the 36 values of P_{ij} only eight should be determined, because the other P_{ij} values are equal to zero or to 1.0. In the first case, P_{ij} = 0 because the corresponding layer pairs are forbidden, whereas in the second case, P_{ij} = 1 because the T^l layers should always follow the T^u layers for definition. If there are no additional constraints for the layer stacking, then, as can be seen in Table 1, only one parameter, P, should be defined. Its value is equal to the total amount of T layers, that is, to 2W. In this case equations of the type $W(T_{60}) = W(T_{-60})\ P\ (T_{-60}\ T_{60}) + W(T^l_{-60})\ P(T^l_{-60}\ T_{60})$, $P(T_{-60}, T_{60}) + P(T_{-60}\ T^u_{60}) = 1$, and $2(W + W_i) = 1$, satisfying the Marcovian statistics are fulfilled.

For a defective $3T$ structural model, each layer should be rotated with respect to the preceding one by 120°, as in the periodic *tv*$3T$ mica. In this case, nine layer types, T_0, T_{120}, T_{240}, T^u_0, T^u_{120}, T^u_{240}, T^l_0, T^l_{120} and T^l_{240} should be used. As in the previous case, one can assume that $W(T_0) = W(T_{120}) = W(T_{240}) = W$ and portions of the other 6 layer types, W_i, are also equal to each other, so that $3W + 6W_i = 1$. Within the constraints described above, only W and W_i values are needed to describe the ± *b*/3 defective $3T$ model. Indeed, in this case the conditional probability of the T_0 (or T_{120}, or T_{240}) layer to follow the T^l_{240} (or T^l_0, T^l_{120}) is equal to 3W, whereas the conditional probability of the T^u_0 (or T^u_{120}, T^u_{240}) layer to follow the T_{240} (or T_0, T_{120}) is equal to $6W_i$. The rest of P_{ij} values differing from 0 and 1 can be found using the equations: $P(T^l_{240}, T_0) + P(T^l_{240}\ T^u_0) = 1$ or $P(T_0\ T_{120}) + P(T_0\ T^u_{120}) = 1$, *etc.*

Thus, in order to describe the ± *b*/3 defective $2M_1$ and $3T$ models, the occurrence probability for each layer type should be defined.

3.2 Interstratification of *cv* and *tv* layers (*tv*/*cv* models)

In a defective *tv*/*cv* $2M_1$ mica model, four layer types, T_{60}, T_{-60}, C^r_{60}, and C^r_{-60}, or T_{60}, T_{-60}, C^l_{60} and C^l_{-60} are interstratified in such a way that the layers in any layer pair, independent of octahedral cation distribution, are rotated with respect to each other by ± 120° as in a periodic *tv*$2M_1$ mica. One may assume, that the occurrence probabilities $W(T_{60}) = W(T_{-60}) = W$ and $W(C^r_{60}) = W(C^r_{-60}) = W_i$. In the case of random interstratification of the layer types having identical azimuthial orientations, the conditional probabilities, P, for the layers T_{60} to follow the layers T_{-60} and C^r_{-60} as well as for the layer T_{-60} to follow the layer T_{60} and C^r_{60} are both equal to 2W. The other nonzero conditional probabilities, P', for the layer C^r_{60} to follow the layers T_{-60} and C^r_{-60} as well as for the layer C^r_{-60} to follow the layers T_{60} and C^r_{60} are both equal to $2W_i$ and $P + P' = 2(W + W') = 1$.

In defective *cv*/*tv* 3*T* mica models, six layer types, T_0, T_{120}, T_{240}, C^r_0, C^r_{120} and C^r_{240} or T_0, T_{120}, T_{240}, C^l_0, C^l_{120} and C^l_{240} are interstratified in such a way that each layer is rotated, with respect to the preceding one, by 120°, counter-clockwise for the first six layer types and clockwise for the second layer sextet. For periodic *cv*3*T* structures, in terms of Zvyagin's notations, the counter-clockwise and clockwise periodic rotations of C^r layers by 120° are represented as 51 13 35 and 51 35 13, respectively, whereas the corresponding rotations of C^l layers, as 15 31 53 and 15 53 31. Let us assume that $W(T_0) = W(T_{120}) = W(T_{240}) = W$ and $W(C^r_0) = W(C^r_{120}) = W(C^r_{240}) = W_i$. As in the previous case, if the layer types having identical azimuthal orientation are interstratified at random then the conditional probabilities, P, for the layer T_0 to follow the layers T_{240} and C^r_{240}, for the layer T_{120} to follow the layers T_0 and C^r_0, and for the layer T_{240} to follow the layers T_{120} and C^r_{120} are all equal to 3W. The other nonzero conditional probabilities, P', are equal to $3W_i$, so that $3(W + W_i) = 1$.

In the general case, additional constraints on the layer sequences may be imposed. For example, the layer types may interstratify with some tendency to segregation. In this case, the P and P' values equal to 3W and $3W_i$ for the random interstratified model may vary within $3W < P \leq 1$ and $3W_i > P' \geq 0$, respectively. The case P = 1 and P' = 0 corresponds to a physical mixture of periodic *tv*3*T* and *cv*3*T* micas. In the case when P > 3W and P' < $3W_i$ the occurrence probabilities for the layer subsequences T_0T_{120} $T_{240}T_0\ldots$ and $C^r_0C^r_{120}C^r_{240}C^r_0$ increase in comparison with those for the layer subsequences in the random model. Simultaneously, the occurrence probabilities of layer subsequences of mixed layer type compositions decrease.

More complex *cv*/*tv*3*T* structural models may consist of nine interstratified layer types, T_0, T_{120}, T_{240}, C^r_0, C^r_{120}, C^r_{240}, C^l_0, C^l_{120} and C^l_{240}. These layers may be distributed at random or with some tendency to segregation.

3.3 Models with partial occupancy of trans-sites

In these models *trans*-sites in the octahedral sheets of $2M_1$ and 3*T* mica models are occupied by Al or Mg cations. These models will be denoted as *m*$2M_1$ and *m*3*T* where m is the occupancy factor equal to 0.10; 0.20, *etc.* atoms per *trans*-site whereas the occupancy of *cis*-sites is equal to 0.95; 0.90, *etc.* atoms per *cis*-site. The atomic coordinates remain the same independent of the occupancy of *trans*- and *cis*-sites.

4. Results

Powder XRD patterns have been calculated for the models described above in the interval 19.0° – 65.0° 2θ. Intensities were calculated with a step equal to 0.02° 2θ. Thicknesses of coherent scattering domains (CSDs) were distributed log-normally and the parameters of this distribution were determined using the mean number of mica layers in CSDs and the regression given by Drits *et al.* (1997) with mean (N) and maximum (N_{max}) numbers of mica layers in CSDs as variable parameters. For all models, $N_{max} = 50$ and N varies from 15 to 12. CSDs were assumed to have disc-like shape, with the diameter of 500 Å. In order to compare XRD patterns calculated for different models, reflection intensities were normalized to those corresponding to reflections whose intensities do not depend on the distribution of octahedral cations over *cis*- and *trans*-sites. These intensities correspond to 20*l*, 13*l* and 11*l* reflections of the $2M_1$ and 3*T* structural models, respectively. In order to estimate the relative difference between the intensities of XRD patterns calculated for two compared models, the standard factor R_{wp} was used.

4.1 Diffraction effects from *m*3*T* and *m*$2M_1$ models

Figure 1 compares XRD patterns calculated for periodic *tv*3*T* and *tv*$2M_1$ micas with those calculated for *m*3*T* and *m*$2M_1$ structural models with m = 0.20 atoms per M1-site. Figure 1 shows that this partial occupancy is accompanied by three principal diffraction features. First, the intensities of 110 and 100 reflections corresponding to the *m*$2M_1$ and *m*3*T* models, respectively, decrease. Second, 11*l*, 02*l* and 10*l* reflections of the *m*$2M_1$ and *m*3*T* models have different sensitivity to redistribution of octahedral cations over *trans*- and *cis*-sites. For example, the intensities of some 02*l*, 11*l* reflections decrease, whereas the intensities of the other reflections are similar for the *m*$2M_1$ and periodic *tv*$2M_1$ micas (Fig.1a). In the case of the *m*3*T* model, the cation redistribution significantly decreases intensities the first four 10*l* reflections with $l < 5$ (Fig. 1b). Third, the intensities of *hkl* reflections located at 2θ > 34° are almost insensitive to the cation distribution. It is obvious that the difference between the compared XRD patterns depends on the occupancy of the *trans*-sites. The calculations have shown that for m = 0.20 atoms, R_{wp} = 7.4 % and 7.5 % for the *m*3*T* and *m*$2M_1$, respectively; but R_{wp} values decrease down to 3.7% for both models for m = 0.10 and increase up to 11.2 % and 11,1 % when m = 0.30.

4.2 Diffraction effects from *tv*/*cv*3*T* models

XRD patterns calculated for *tv*/*cv*3*T* models consisting of different amounts of interstratified *cv* and *tv* layers and differing from each other in the modes in the layer distri-

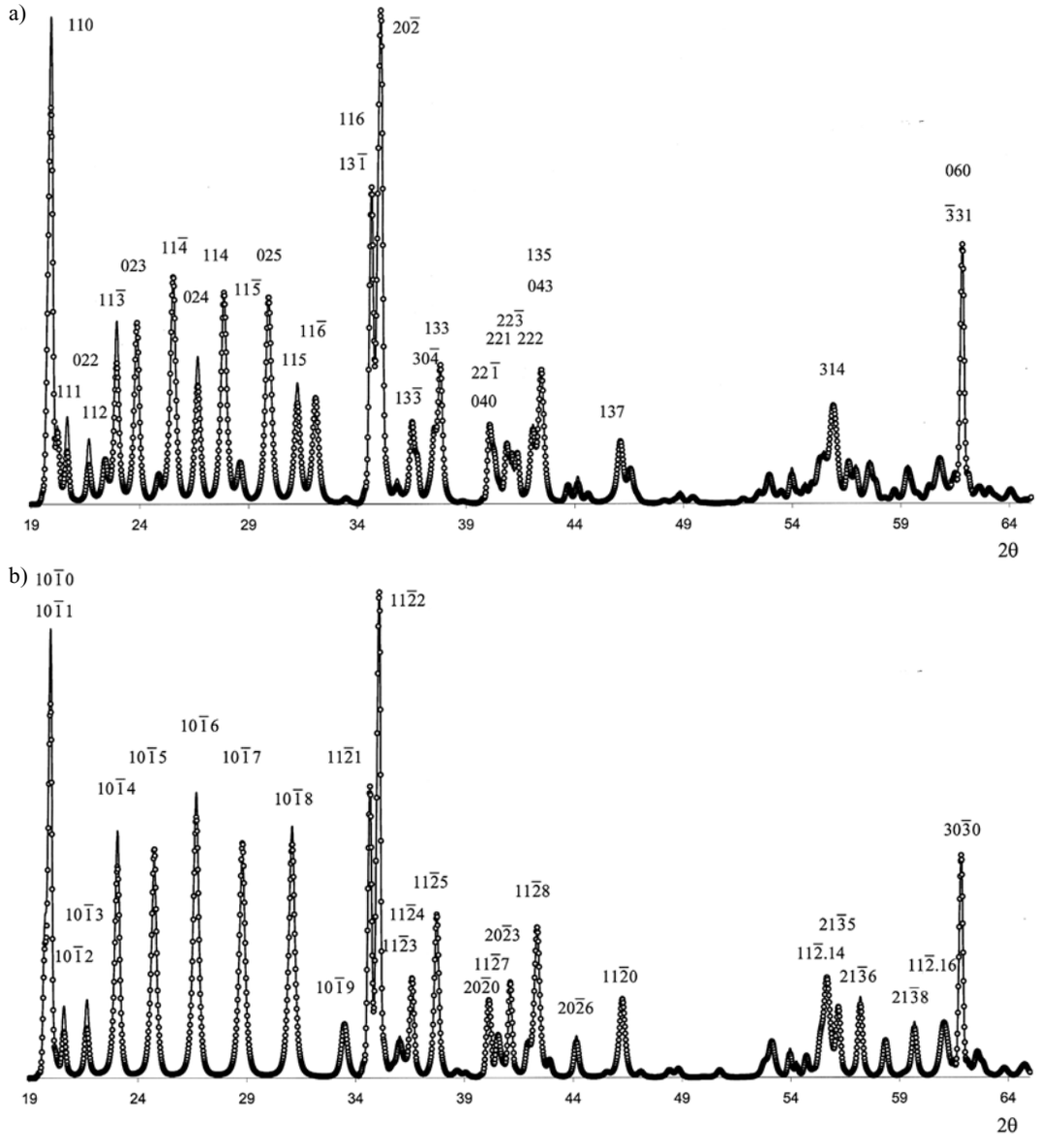

Fig. 1. Comparison of XRD patterns calculated for the $tv2M_1$ (solid line) and $m2M_1$ models (a) as well as for the $tv3T$ (solid line) and $m3T$ models (b). m = 20 %. (N = 15).

bution were compared with that calculated for a periodic $tv3T$ mica. It was found that the XRD patterns of the $tv3T$ and $cv/tv3T$ containing 10 % of cv layers are almost undistinguishable (R_{wp} = 6.3 %). Further increase of cv layers is accompanied more significant modification (Fig. 2a). In particular, intensity of 102 and 103 reflections dramatically decreases whereas 106 reflection becomes more strong in comparison with corresponding reflections of the $tv3T$. Accordingly, the R_{wp} values increase and equal to 9.0 %, 12.5 % and 15.3 % when amount of cv layers are equal to 20 %, 30 % and 40 %. It is remarkable, however, that segregation of the interstratified layer types in $tv/cv3T$ models significantly decreases the difference between XRD patterns calculated for the models containing different amount of cv layers. For example the XRD patterns corresponding to $cv/tv3T$ models consisting of 20 % and 10 % cv layers almost coincide (R = 2.1%) when layers in both models are distributed with P = 0.90. Similarly, XRD patterns calculated for $tv/cv3T$ models containing 20, 30 and 40 % of cv layers in which the layer types are distributed with P = 0.80 are also very similar. Comparison of these patterns shows that for any two patterns the R_{wp} value does not exceed 4.3 %. Therefore, it is not surprising that XRD patterns calculated for a segregated $tv/cv3T$ model containing 40 % of cv layers remain quite similar to that of $tv3T$ mica except for $10l$ reflections with $l \leq 4$ (Fig. 2b). For the compared XRD patterns, R_{wp} values vary from 7.5 to 10.8 % depending on the cv layer amount.

Redistribution of $10l$ reflections observed for $cv/tv3T$ models consisting in nine interstratified layer types, T_0, T_{120}, T_{240}, C^l_0, C^l_{120}, C^l_{240}, C^r_0, C^r_{120}, and C^r_{240} is quite similar to that observed for the $cv/tv3T$ models containing six layer types. However, increase of cv layers in these nine-component systems is accompanied more significant decreasing

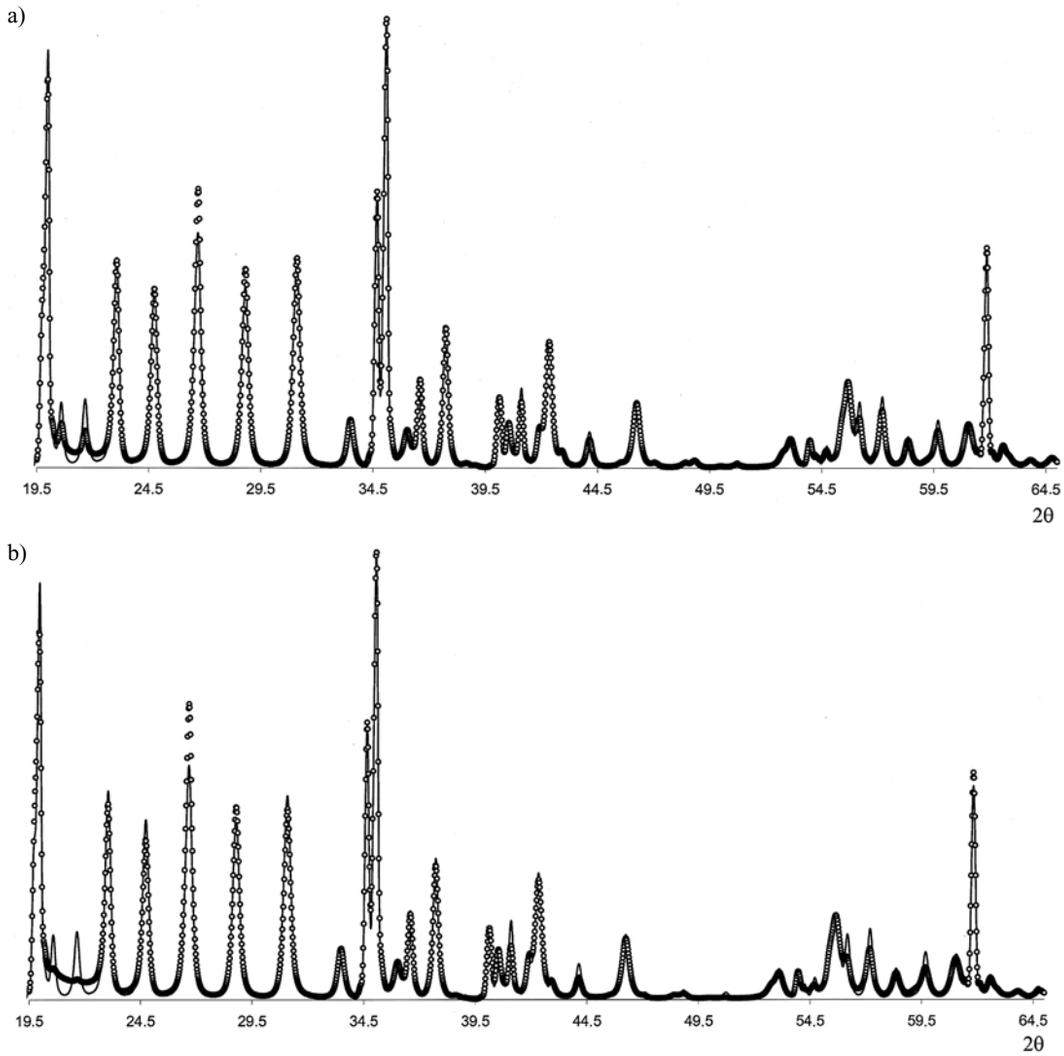

Fig. 2. Comparison of XRD patterns calculated for the *tv*3*T* (solid line, N = 12) and for the *cv*/*tv*3*T* models containing 20 % (a) and 40 % (b) of *cv* layers (N = 15). The XRD pattern (b) corresponds to the *cv*/*tv*3*T* in which the layer types distribution has a strong tendency to segregation (see text).

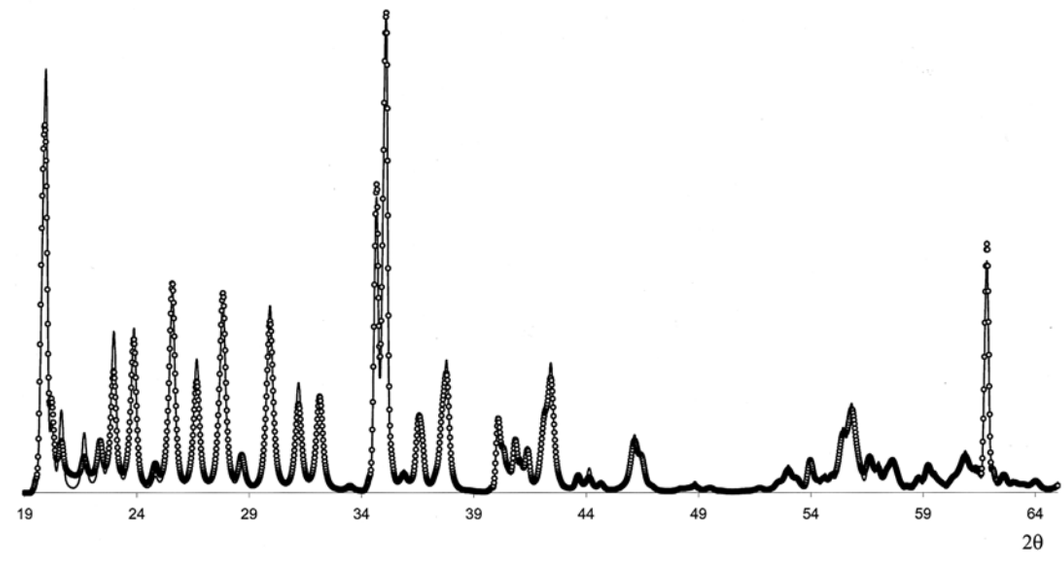

Fig. 3. Comparison of XRD patterns calculated for the defect-free $tv2M_1$ (solid line, N = 12) and for the $cv/tv2M_1$ models containing 20 % of *cv* layers (N = 15).

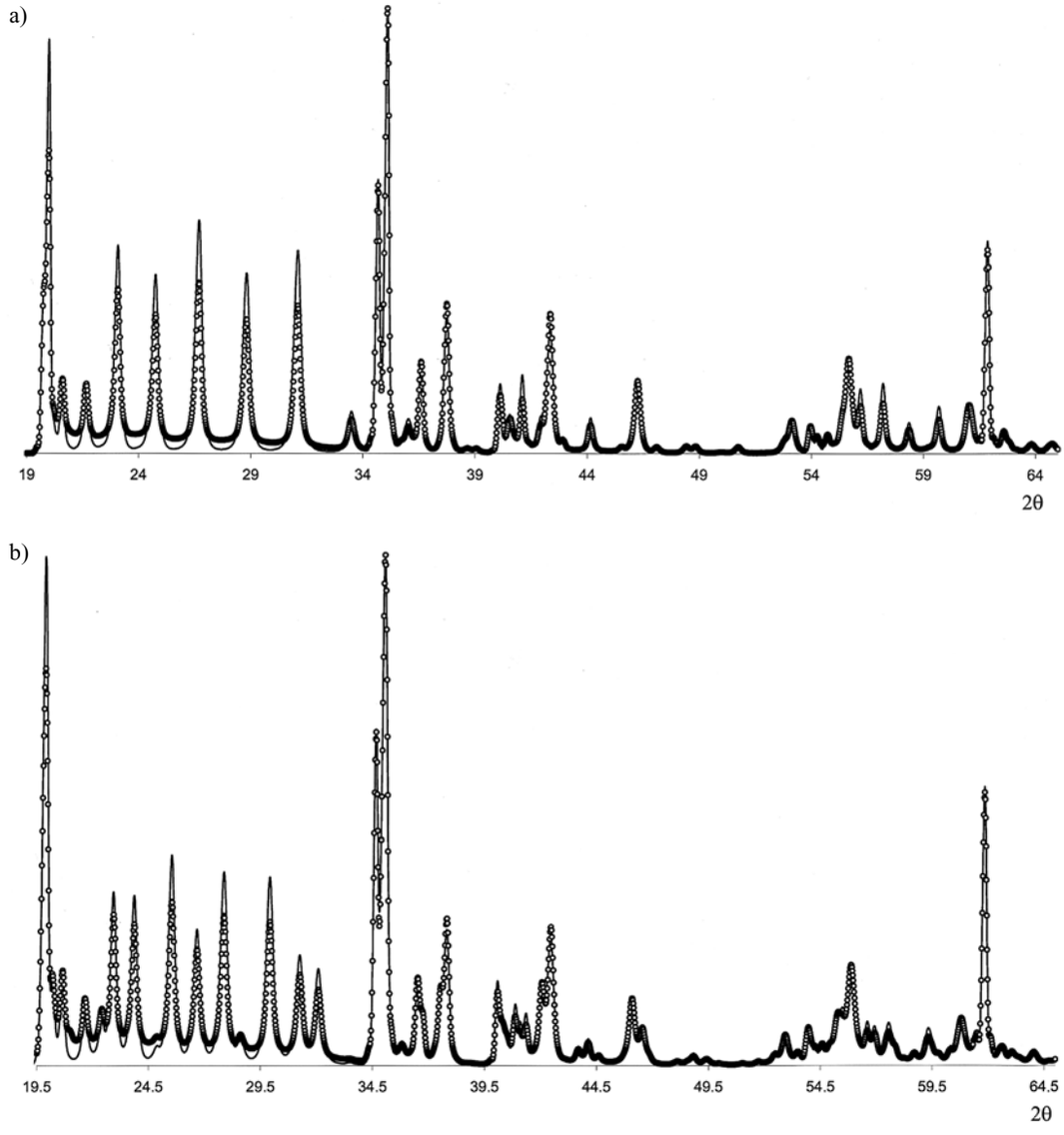

Fig. 4. Comparison of XRD patterns corresponding to the *tv*3*T* (a) and *tv*2M_1 (b) (solid lines)and to the ± *b*/3 disordered 3*T* and 2M_1 models containing 20 % of defective T^u and T^l layers (N = 15) (see text).

of 10*l* reflections with $l < 5$. Therefore, R_{wp} values increase up to 10.0, 14.2 and 17.8 % when total amount of *cv* layers are equal to 20, 30 and 40 %.

4.3 Diffraction effects from *tv*/*cv*2M_1 model

XRD patterns calculated for *tv*/*cv*2M_1 models containing different total amounts of *cv* layers, W(C), were compared with those calculated for periodic *tv*2M_1 mica structures. An increase in *cv* layers is accompanied mainly by a redistribution of 02*l*, 11*l* reflections intensities. In particular, the intensities of 110, 111, 022, $11\bar{3}$, 024 and 115 reflections decrease, whereas the other reflections are not so sensitive to variations in *cv* layers content. However, as in the case of *cv*/*tv*3*T* models when the amounts of *cv* layers are relatively small (*e.g.* W(C) = 10 %), the XRD patterns of the *tv*/*cv*2M_1 and pure *tv*2M_1 are practically undistinguishable (R_{wp} = 7.3 %). Figure 3 shows that even when W(C) = 20 % the difference between the compared XRD patterns remains relatively small (R_{wp} = 9.7 %). For *tv*/*cv*2M_1 models with W(C) > 25 %, the intensity redistribution becomes stronger, and the models may be identified taking account of very low intensities of 111, 022, 112 and $11\bar{3}$ reflections.

As mentioned above, the interstratification of *cv* and *tv* layers is accompanied by the interstratification of different interlayer translations equal to –0.383*a* and –0.3085*a* which are associated with *tv* and *cv* layers, respectively. It is well known that the remarkable feature of diffraction effects is their ability to average interstratified structural parameters (Méring, 1949; Drits & McCarty, 1996). Similar effects are observed in the case of *tv*/*cv*2M_1 mica models. Both layer types have two azimuthal orientations rotated with respect to each other by 120°. Along each of these directions, as well as along the resulting *a* axis, the two interlayer translations are interstratified in proportion determined by the amount of *tv* and *cv* layers. Therefore diffraction averages interstratified –0.383*a* and –0.3085*a*

translations. It means that each given *tv*/*cv*2M_1 structure is characterized by a statistically weighted interlayer displacement equal to T_{ef} = –0.383W(T) – 0.3085W(C). Therefore, the positions of *hkl* reflections in XRD patterns of the *tv*/*cv*2M_1 models depend on the contents of the interstratified layers. Moreover, for each given *tv*/*cv*2M_1 structure, the positions of *hkl* reflections should coincide with those of *tv*2M_1 structure, for which the projection of the *c* axis on the *ab* plane (*c* cos *β*/*a*) is equal to T_{ef} calculated for a given *tv*/*cv* ratio. The validity of these considerations is confirmed by full coincidence of *hkl* reflections' positions in the compared XRD patterns shown in Fig. 3. In particular, the XRD patterns of *tv*2M_1 micas were calculated with *c* cos *β*/*a* equal to –0.3756*a*, –0.3681*a* and –0.3607*a* in order to be compared with the XRD patterns of the *tv*/*cv*2M_1 models containing 10 %, 20 % and 30 % of *cv* layers.

4.4 Diffraction effects from ± *b*/3 disordered models

XRD patterns calculated for the ± *b*/3 disordered 3*T* and 2M_1 models having 10 % and 20 % of defective T^u and T^l layers were compared with XRD patterns of defect-free *tv*3*T* and *tv*2M_1 micas. An increase in the amount of defective layers is accompanied by increasing background within of 2θ from 19° to 34° and decreasing intensities of *hkl* reflections located in this diagnostic interval of 2θ. Note that *hkl* reflections located at 2θ > 34° have low sensitivity to variation in the "defective" layer content. At low amount of T^u and T^l layers (*e.g.* 10 %), modifications of the XRD patterns are relatively small and R_{wp} factor is equal to 12.8 % and 9.0 % when the XRD patterns of the defective 3*T* and 2M_1 structural models are compared with those of the defect-free *tv*3*T* and *tv*2M_1. However, Fig. 4a and 4b shows that the difference between the compared XRD patterns increases dramatically when the amount of the "defective" layers is equal to 20 % and R_{wp} values are equal to 22.2 % and 16.0 for the 3*T* and 2M_1 models.

5. Discussion

The results of the calculations allow us to answer the question of Pavese *et al.* (2001) concerning the origin of partial occupancy of *trans*-sites in the phengite samples, as well as to reveal certain problems which should be taken into account to determine the actual structure of fine-dispersed dioctahedral 3*T* and 2M_1 mica polytypes using their powder XRD patterns. The presence of the T^u and T^l layers in the 2M_1 and 3*T* structures is accompanied by displacements of some octahedral and tetrahedral cations as well as oxygen atoms from their standard positions to those which are unoccupied in the defect-free polytypes. The contribution of these "shifted" atoms disturbs the reflections' intensities. Due to the ability of diffraction to average structural parameters, a XRD pattern from the ± *b*/3 disordered mica structure should be treated in terms of the unit cell in which occupancies can appear in positions generated by the structural disorder. Pavese *et al.* (2001) assumed that the scaling of the structural factors should greatly smooth the effect of the contribution of the shifted atoms to the reflections' intensities, but they did not estimate this effect quantitatively.

Analysis of the XRD patterns calculated from the ± *b*/3 disordered 2M_1 and 3*T* models shows that the main contribution to the modification of the patterns results not from the partial occupancy of *trans*-sites in the defective T^u and T^l layers but from the disordered displacements of the tetrahedral sheets and oxygen atoms of the octahedral sheets in these layers by ± *b*/3. Indeed, as shown in Fig. 1, partial occupancy of *trans*-sites decreases the intensities of only some of the 11*l*, 02*l* and 10*l* reflections of the *m*2M_1 and *m*3*T* models and does not change the background. In contrast, the ± *b*/3 layer displacements decrease the intensities of all 11*l*, 02*l* and 10*l* reflections and dramatically increase the background (Fig. 4). These features are typical for the XRD patterns of the ± *b*/3 disordered phyllosilicates (Drits & Tchoubar, 1990; Drits *et al.*, 1984). In particular, to get a fractional occupancy of *trans*-sites of about 20 %, the ± *b*/3 defective 3*T* structure should contain similar amounts of T^u and T^l layers. As a consequence, the background increases and 10*l* reflections' intensities decrease so dramatically that the scaling of the structural factors cannot smooth this effect (Fig. 4).

Even when the amounts of T^l and T^u layers in the 2M_1 and 3*T* micas are rather small, and corresponding XRD patterns can be used for the Rietveld refinement the presence of the ± *b*/3 disorder can be detected using the fact that background and intensities of 11*l*, 02*l* and 10*l* reflections located in the interval 19°-34° 2θ are most sensitive to this disorder. Therefore, R_{wp} factors determined for two different intervals of the XRD pattern (19°- 34°2θ and 2θ ≥ 34°2θ) should be significantly different if the intensity in each interval is scaled using reflections which are not sensitive to the ± *b*/3 disorder. In this case, R_{wp} factor for the first interval should be much higher than that for the second one. For example, comparison of XRD patterns calculated for 3*T* model containing 10 % of the defective layers and for *tv*3*T* model shows R_{wp} = 14.7 % for the first and R_{wp} = 8.55 % for the second interval.

Diffraction effects from *tv*/*cv*2M_1 and *tv*/*cv*3*T* models are, in general, quite similar to those observed for *m*2M_1 and *m*3*T* models especially when W(C) = m. Indeed, an increase in the *cv*-layer amount, as well as in the occupancy of *trans*-sites in the models is accompanied by decreasing intensity of reflections having the same *hkl* indices. This similarity does not mean that the XRD patterns of the *tv*/*cv*3*T* and *m*3*T* completely coincide because average overlapping of atomic positions of the interstratified *cv* and *tv* layers is not equivalent to the atomic sites of the layers with a partial occupancy of *trans*-sites. It means, however, that the main modification of the XRD patterns from the *tv*/*cv*3*T* structures appears as a result of the partial occupancy of *trans*-sites mimicking the presence of *cv* layers in the actual structure. For example, 20 % of *cv* layers in the *tv*/*cv*3*T* (Fig. 2b) and 20 % atoms in *trans*-sites in the *m*3*T* (Fig. 1a) result in a similar decrease in the intensities of 10*l* reflections having the same *l* values. Similar diffraction features are observed for *tv*/*cv*2M_1 models. For example, comparison of Fig. 1b and 3 shows that an increase in the

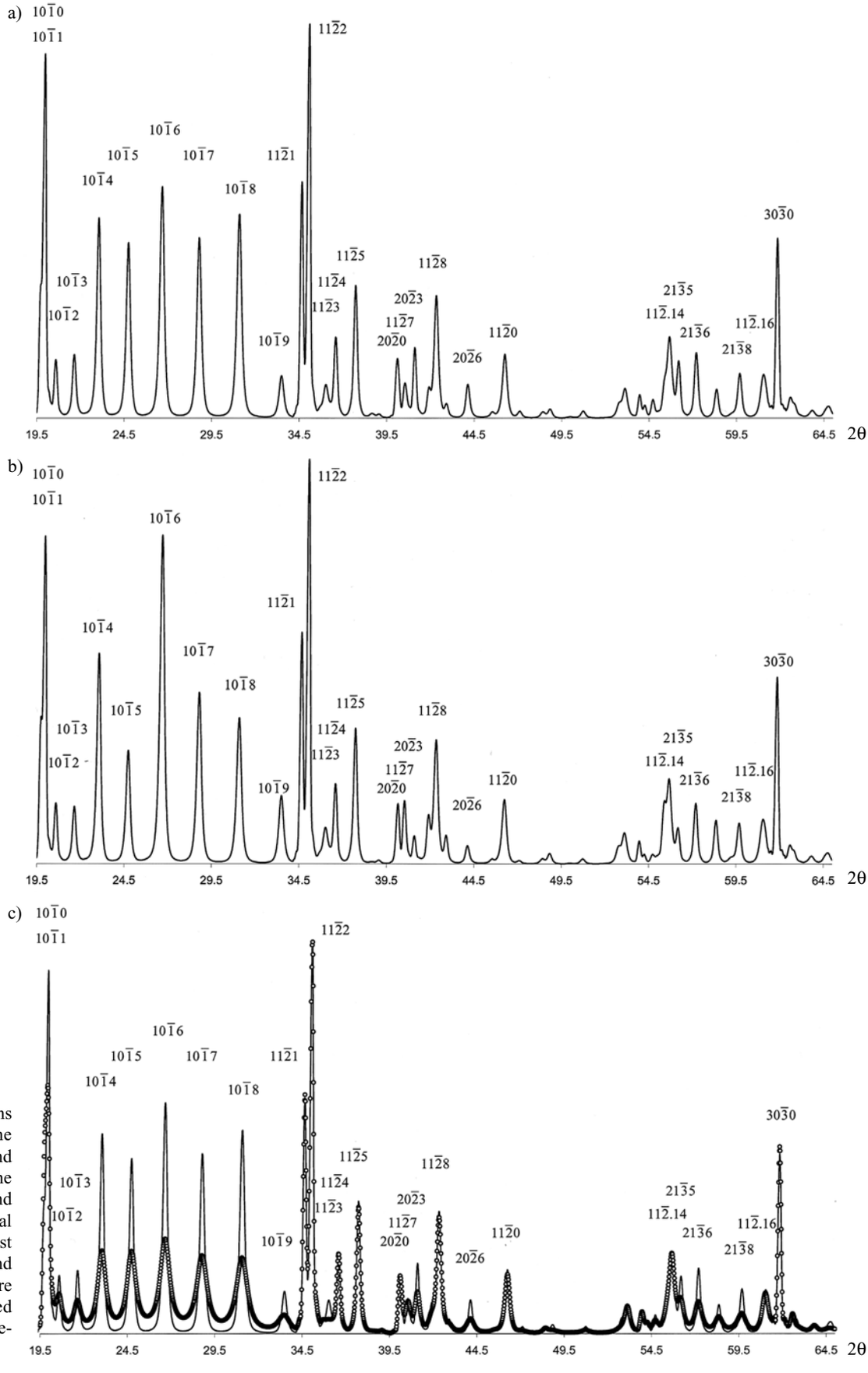

Fig. 5. XRD patterns calculated for the *tv*3*T* (a), *cv*3*T* (b) and as well as for the *tv*3*T* (solid line) and *cv*/*tv*3*T* (c) structural models. In the last one 80 % of T and 20 % of C^r layers are clockwise rotated with respect to preceding one by 120°.

amount of *cv* layers in the *tv*/*cv*2M_1 structures as well as partial occupancy of *trans*-sites in the *m*2M_1 ones are accompanied by similar decrease in the intensities of reflections having the same *hkl* indices. A remarkable diffraction feature of the *tv*/*cv*2M_1 is that the positions of *hkl* reflections observed in each XRD pattern can be described in terms of the unique unit cell despite the interstratification of two different interlayer translations. The fact that in this cell, the effective interlayer displacement along the *a* axis, $|c\cdot\cos\beta/a|$, decreases with the amount of *cv* layers, can be used as an additional criterion for the identification of the *tv*/*cv*2M_1 micas, taking into account that $|c\cdot\cos\beta/a| \geq 0.383$ for micas of muscovite-phengite composition (Bailey, 1984).

Qualitative identification of the *tv*/*cv*3*T* and *tv*/*cv*2M_1 micas should be especially problematic in the following cases: low content of *cv* layers (< 10 %); a strong tendency of *cv* and *tv* layers to be segregated in *tv*/*cv*3*T*; very small sizes of CSDs; presence of rotational stacking faults. In the first case, the XRD patterns from the interstratified and defect-free 3*T* and 2M_1 models are quite similar or even undistinguishable. As was mentioned, a strong tendency to segregation of the layer types in the *tv*/*cv*3*T* significantly decreases the difference between the XRD patterns corresponding to the models having quite different amounts of *cv* layers. The main reason is that XRD patterns corresponding to the periodic $T_0T_{120}T_{240}T_0\ldots$ and $C^r_0C^r_{120}C^r_{240}C^r_0\ldots$ layer sequences (space group $P3_112$) are rather similar. As can be seen in Fig. 5a and 5b, they have the same positions and shapes of *hkl* reflections and differ from each other only by lower intensities of 105 and 108 reflections corresponding to the *cv*3*T* structure. The significant difference between the intensities of the 106 reflections in the compared XRD patterns has no diagnostic meaning because of their overlapping with 006 reflection. Finally, small sizes of CSDs and stacking faults are accompanied by broadening of *hkl* reflections and decreasing difference between the compared XRD patterns.

However, when the amount of *cv* layers in *tv*/*cv*2M_1 and *tv*/*cv*3*T* is rather high (> 20 %) and they are distributed "at random" among *tv* layers, then the following criteria can be used for their identification: absence or extremely low intensities of 102 and 103 reflections for *tv*/*cv*3*T* (Fig. 2) and of 111 and 022 ones for *tv*/*cv*2M_1 (Fig. 3). Because of the absence of 102 and 103 reflections one may suspect that a dioctahedral mica sample given as a *tv*3*T* standard in the textbooks (Brindley, 1980; Bailey, 1980, 1984) consists of interstratified *cv* and *tv* layers.

Because both positions and profiles of *hkl* reflections of the *tv*/*cv*2M_1 and *tv*/*cv*3*T* models are the same as those of periodic and defect-free structures, the Rietveld technique may be used to refine mica samples consisting of *tv* and *cv* layers using both X-ray and neutron diffraction. However, in the general case, along with conventional *tv* mica polytypes, initial models for the Rietveld refinement should include a partial occupancy of *trans*-sites. This requirement may have a practical meaning. It is well known that cation ordering over the tetrahedral and octahedral sites in dioctahedral micas is the subject of many publications (see review in Pavese, 2002). Special interest to this problem for phengites is derived from the assumption that the stability of 2M_1 and 3*T* phengites is related to the cation ordering occurring in T and M sites. However, it would be difficult to achieve reliable results in terms of cation partitioning if the actual structure of phengite samples consists of *tv* and *cv* layers.

Let us consider some crystal-chemical features of the *tv*3*T*, *cv*3*T* and *tv*/*cv*3*T* structures which, most probably, make their XRD patterns similar. As was mentioned, in the *tv*3*T*, *cv*3*T* and *cv*/*tv*3*T* structures, T and/or C^r layers are counter-clockwise rotated with respect to the preceding one by 120°. Therefore, in the normal projection on the *ab* plane one of the two sets of symmetrically independent octahedral cations of the subsequent T and/or C^r layer almost superimpose on the OH groups located in the lower oxygen plane of the octahedral sheet of the preceding layer. The other half of the octahedral cations, as well as vacant octahedral sites of the subsequent layer, almost coincide with the tetrahedral cations of the lower sheet of the preceding layer. Such homogeneous disposition of the octahedral and tetrahedral cations, as well as OH groups in the adjacent layers is more favourable in comparison with a cation distribution when in the projection on the *ab* plane all octahedral cations of the subsequent layer superimpose on the tetrahedral cations of the following layer. Such an unfavourable mutual cation disposition takes place in *cv*/*tv*3*T* mica models in which the subsequent T or C^r layers are clockwise rotated with respect to the preceding one by 120°. In such structures, mutual dispositions of octahedral and tetrahedral cations in the adjacent layer pairs are different. In particular, in the projection on the *ab* plane, all octahedral cations of the following layer in the $C^r - C^r$ and $C^r - T$ layer pairs almost coincide with tetrahedral cations of the lower sheet of the preceding layer. In contrast, for layer pairs T – T and T – C^r, only half of the octahedral cations overlap with tetrahedral ones. That is why the XRD patterns corresponding to such structural models (Fig. 5c) are quite similar to those characteristic for disordered micas containing rotational stacking faults.

Acknowledgements: V.A. Drits and B.A. Sakharov thanks B.B. Zviagina for comments and the English corrections, E.V. Pokrovskaya for the paper preparation help. This work was supported by the Russian Science Foundation, grant 01-05-64486.

References

Bailey, S.W. (1980): Structures of layer silicates. *in* "Crystal structures of clay minerals and their X-ray identification". Eds: G.W. Brindley & G. Brown, Mineralogical Society, London SW7 5HR, 495p.

— (1984): Crystal chemistry of the true mica: *in* "Micas, Reviews in Mineralogy". S.W. Bailey, ed., Mineralogical Society of America, 13-66.

Brigatti, M.F. & Guggenheim, S. (2000): Mica crystal chemistry and the influence of intensive variables on atomistic models. *Advanced on Micas* (*Problems, Methods, Applications in Geodynamics*). Accademia Nazionale dei Lincei, Roma, Italy, 29-56.

Brigatti, M.F., Frigieri, P., Poppi, L. (1998): Crystal-chemistry of Mg-, Fe-bearing muscovites $2M_1$. *Am. Mineral.*, **83**, 775-785.

Brigatti, M.F., Frigieri, P., Ghezzo, C., Poppi, L. (2000): Crystal chemistry of Al-rich biotites coexisting with muscovites in peraluminous granites. *Am. Mineral.*, **85**, 436-448.

Brindley, G.W. (1980): Order-disorder in clay mineral structures. *In*: Brindley, G.W. and Brown, G. eds., "Crystal structures of clay minerals and their X-ray identification". *Mineral. Society, London,* 125-196.

Cuadros, J. & Altaner, S.P. (1998): Characterization of mixed-layer illite-smectite from bentonites using microscopic, chemical and X-ray methods: constrains on the smectite-to-illite transformation mechanism. *Am. Mineral.*, **83**, 762-774.

Drits, V.A. & McCarty, D. (1996): A simple technique for a semi-quantitative determination of the *trans*-vacant and *cis*-vacant 2:1 layer contents in illites and illite-smectites. *Am. Mineral*, **81**, 852-863.

Drits, V.A. & Tchoubar, C. (1990): "X-ray Diffraction of Disordered Lamellar Structures. Theory and Application to Microdivided Silicates and Carbons". Springer Verlag, 242 pp.

Drits, V.A., Plançon, A., Sakharov, B.A., Besson, G., Tsipursky, S.I., Tchoubar, C. (1984): Diffraction effects calculated for structural models of K-saturated montmorillonite containing different types of defects. *Clay Minerals*, **19**, 541-562.

Drits, V.A., Weber, F., Salyn, A., Tsipursky, S. (1993): X-ray identification of 1*M* illite varieties. *Clays and Clay Minerals*, **28**, 185-207.

Drits, V.A., Salyn, A.L., Sucha, V. (1996): Dynamic and mechanism in the structural transformation of illite-smectites from Dolna Ves hydrothermal deposits. *Clays and Clay Minerals*, **44**, 181-190.

Drits, V.A., Środoń, J., Eberl, D.D. (1997): XRD measurement of mean illite crystallite thickness: Reappraisal of the Kübler index and the Scherrer equation. *Clays and Clay Minerals*, **45**, 461-475.

Drits, V.A., Lindgreen, H., Salyn, A.L., Ylagan, R., McCarty, D.K. (1998a): Semiquantitative determination of *trans*-vacant and *cis*-vacant 2:1 layers in illites and illite-smectites by thermal analysis and X-ray diffraction. *Am. Mineral.*, **83**, 31-73.

Drits, V.A., Lanson, B., Gorshkov, A.I., Manceau, A. (1998b): Sub- and super-structure of four-layer Ca-exchanged birnessite. *Am. Mineral.*, **83**, 97-118.

Drits, V.A., Sakharov, B.A., Dainyak, L.G., Salyn, A.L., Lindgreen, H. (2002): Structural and chemical heterogeneity of illite-smectites from Upper Jurrasic mudstones of East Greenland related to volcanic and weathered parent rocks. *Am. Mineral.*, **87**, 1590-1607.

Ey, F. (1984): Un exemple de gisement d'uranium sous discordance: les minéralisations protérozoiques de Cluff Lake, Saskatchewan, Canada: Thèse doctorale, Université Louis Pasteur, Strasbourg 1.

Halter, G. (1988): Zonalité des altérations dans l'environement des gisements d'uranium associée à la discordance du Protérozoique moyen (Saskatchewan, Canada): Thèse doctorale, Université Louis Pasteur, Strasbourg 1.

Horton, D. (1983): Argillitic alteration associated with the amethyst vein system, Creede Mining District, Colorado. Ph.D. dissertation, University of Illinois, Urbana-Champaign.

Lanson, B., Drits, V.A., Silvester, E., Manceau A. (2000): Structure of H-exchanged hexagonal birnessite and its mechanism of formation from Na-rich monoclinic buserite at low pH. *Am. Mineral.*, **85**, 826-838.

Lanson, B., Drits, V.A., Gaillot, A-C., Silvester, E., Plancon, A., Manceau, A. (2002): Structure of heavy metal sorbed birnessite: Part I. Results from X-ray diffraction. *Am. Mineral.*, **87**, 1631-1645.

Lindgreen, H., Drits, V.A., Sakharov, B.A., Salyn, A.L., P.Wrang, Dainyak, L.G. (2000): Illite-smectite structural changes during metamorphism in black Cambrian Alum shales from the Baltic area. *Am. Mineral.*, **85**, 1223-1238.

Manceau, A., Drits, V.A., Silvester, E.J., Bartoli, C., Lanson, B. (1997): Structural mechanism of Co^{3+} oxidation by the phyllomanganate buserite. *Am. Mineral.*, **82**, 1150-1175.

Manceau, A., Lanson, B., Drits, V.A., Chateigner, D., Gates, W.P., Wu, J., Huo, D., Stucki, J.W. (2000): Oxidation-reduction mechanism of iron in dioctahedral smectites. I. Crystal chemistry of oxidized reference nontronites. *Am. Mineral.*, **85**, 133-152.

McCarty, D.K. & Reynolds, R.C. (1995): Rotationally disordered illite-smectite in Paleozoic K-bentonites. *Clays and Clay Minerals*, **43**, 271-284.

—, — (2001): Three-dimensional crystal structures of illite-smectite minerals in Paleozoic K-bentonites from the Appalachian basin. *Clays and Clay Minerals*, **49**, 24-35.

Mering, J. (1949): L'interférence des rayons X dans les systèmes à stratification désordonnée. *Acta Cryst.*, **2**, 371-377.

Mering, J. & Oberlin, A. (1967): Electron-optical study of smectites. *Clays and Clay Minerals*, **15**, 3-25.

Nespolo, M. (2001): Perturbative theory of mica polytypism. Role of the M2 layer in the formation of inhomogeneous polytypes. *Clays and Clay Minerals*, **49**, 1-23.

Nespolo, M. & Ferraris, G. (2001): Effects of the stacking faults on the calculated electron density of mica polytypes – the Ďurovič effect. *Eur. J. Mineral.*, **13**, 1035-1045.

Noe, D.C. & Veblen, D.R. (1999): HRTEM analysis of dislocation cores and stacking faults in naturally deformed biotite crystals. *Am. Mineral.*, **84**, 1925-1931.

Pavese, A. (2002): Neutron powder diffraction and Rietveld analysis; application to crystal-chemical studies of minerals at non-ambient conditions. *Eur. J. Mineral.*, **14**, 241-249.

Pavese, A., Ferraris, G., Pishedda, V., Fauth, F. (2001): M1-site occupancy in $3T$ and $2M_1$ phengites by low temperature neutron powder diffraction: reality or artifact? *Eur. J. Mineral.*, **13**, 1071-1078.

Plançon, A. (1981): Diffraction by layer structures containing different kinds of layers and stacking faults. *J. Appl. Cryst.*, **14**, 300-304.

Plançon, A. & Tchoubar, C. (1977): Determination of structural defects in phyllosilicates by X-ray powder diffraction. I. Principle of calculation of the diffraction phenomenon. *Clays and Clay Minerals,* **25**, 430-435.

Plançon, A., Giese, R.F., Snyder, R., Drits, V.A., Bookin, A.S. (1989): Stacking faults in the kaolin-group minerals: Defect structures of kaolinite. *Clays and Clay Minerals*, **37**, 203-210.

Reynolds, R.C., Jr. (1993): Three-dimensional X-ray diffraction from disordered illite: simulation and interpretation of the diffraction patterns. *In*: "Computer Applications to X-ray Diffraction Methods" (R.C. Reynolds and J. Walker, eds.). Clay Minerals Society, Workshop Lectures 5, 44-78.

Reynolds, R.C. & Thompson, C.H. (1993): Illites from the Postam sandstone of New York, a probable noncentrosymmetric mica structure. *Clays and Clay Minerals*, **41**, 66-72.

Sakharov, B.A., Naumov, A.S., Drits, V.A. (1982): X-ray diffraction by mixed-layer structures with random distribution of stacking faults. *Doklady Akademii Nauk SSSR,* **265,** 339-343**.**

Sakharov, B.A., Besson, G., Drits, V.A., Kameneva, M.Y., Salyn A.L., Smoliar, B.B. (1990): X-ray study of the nature of stac-

king faults in the structure of glauconites. *Clay Minerals*, **25**, 419-435.

Sassi, P.F., Guidotti, C., Rieder, M., De Pieri, R. (1994): On the occurrence of methamorphic $2M_1$ phengites: some thoughts on polytypism and crystallization conditions of $3T$ phengites. *Eur. J. Mineral.*, **6**, 151-166.

Tsipursky, S.I. & Drits, V.A. (1984): The distribution of octahedral cations in the 2:1 layers of dioctahedral smectites studied by oblique texture electron diffraction. *Clay Minerals*, **19**, 177-193.

Warshaw, C.M. (1959): Experimental studies of illites. *Clays and Clay Minerals*, **7**, 303-316.

Ylagan, R.F., Altaner, S.P., Pozzuoli, A. (2000): Reaction mechanisms of smectite illitization associated with hydrothermal alteration from Ponza island, Italy. *Clays and Clay Minerals*, **48**, 610-631.

Zvyagin, B.B. (2001): Current problems with the nomenclature of phyllosilicates. *Clays and Clay Minerals*, **49**, 492-499.

Zvyagin, B.B., Rabotnov, V.T., Sidorenko, O.V., Kotelnikov, D.D. (1985): Unique mica consisting of noncentrosymmetric layers. *Izvestiya Akademii Nauk S.S.S.R*, *Seriya Geologicheskaya*, **35**, 121-124 (in Russian).

Received 4 April 2003
Modified version received 11 September 2003
Accepted 15 October 2003